Elastic rebound following the Kocaeli earthquake, Turkey, recorded using synthetic aperture radar interferometry

Larry Mayer   Department of Geosciences, University of Arizona, Tucson, Arizona 85721, USA
Zhong Lu   Raytheon STX, U.S. Geological Survey, Eros Data Center, Sioux Falls, South Dakota 57198, USA

ABSTRACT

A basic model incorporating satellite synthetic aperture radar (SAR) interferometry of the fault rupture zone that formed during the Kocaeli earthquake of August 17, 1999, documents the elastic rebound that resulted from the concomitant elastic strain release along the North Anatolian fault. For pure strike-slip faults, the elastic rebound function derived from SAR interferometry is directly invertible from the distribution of elastic strain on the fault at criticality, just before the critical shear stress was exceeded and the fault ruptured. The Kocaeli earthquake, which was accompanied by as much as ~5 m of surface displacement, distributed strain ~110 km around the fault prior to faulting, although most of it was concentrated in a narrower and asymmetric 10-km-wide zone on either side of the fault. The use of SAR interferometry to document the distribution of elastic strain at the critical condition for faulting is clearly a valuable tool, both for scientific investigation and for the effective management of earthquake hazard.

INTRODUCTION

Direct detailed measurement of elastic rebound for the Kocaeli earthquake using synthetic aperture radar (SAR) interferometry documents for the first time the critical strain conditions for the North Anatolian fault at the time of rupture, and a new application for SAR interferometry. The magnitude (Mw) 7.4 Kocaeli earthquake (Fig. 1) occurred on August 17, 1999; its hypocenter was 10–15 km and the epicenter was located only 70 km southeast of Istanbul (Barka, 1999). The nearly pure strike-slip earthquake ruptured 120 km of the North Anatolian fault; the maximum measured displacement was that of a country road, 5 m, and the typical slip was 2.5–4.5 m in a right-lateral sense (Barka, 1999). The fault rupture consisted largely of long east-west–oriented strike-slip sections linked by short (1 km long) right-stepping normal faults. The rupture occurred on a section of the North Anatolian fault that represented the continued westward migration of ground-rupturing earthquakes, starting with the 1939 Erzincan earthquake (Stein et al., 1997).

Direct observation of elastic strain over a widespread area occurring within short time periods (years) is difficult because small spatial strain gradients measured using conventional geodetic surveying techniques are difficult to resolve. Although modern Global Positioning System (GPS) measurement precision would allow these small strains to be detected, the density of the GPS arrays required for spatially detailed deformation studies over a large area is commonly prohibitive unless there is a strategy for knowing how to set up such a survey. Thus, despite the fact that earthquakes are generated from the release of elastic strain energy that accumulates around the fault, we have not had an image of the elastic strain as seen directly through the elastic rebound until now.

INTERFEROMETRY

Interferometric synthetic aperture radar (InSAR) has become an important geodetic imaging technique used to map deformation of Earth's surface (e.g., Massonnet and Feigl, 1998). InSAR utilizes two synthetic aperture radar (SAR) images of the same area on the ground, but acquired at different dates, in order to detect any ground deformation that might have occurred during the intervening period. The detection of surface deformation is possible because InSAR measures phase differences between two SAR images that result from the difference in the round-trip path length from the satellites to the same ground point. The phase difference can be further processed to map ground deformation over large areas at a horizontal pixel resolution of 20 m with centimeter to subcentimeter vertical precision.

To study ground deformation associated with the August 17, 1999, Kocaeli earthquake, we performed two-pass InSAR using SAR data acquired by the European Space Agency ERS-2 satellites (e.g., Rosen et al., 1996; Massonnet and Feigl, 1998; Lu et al., 2000). ERS-
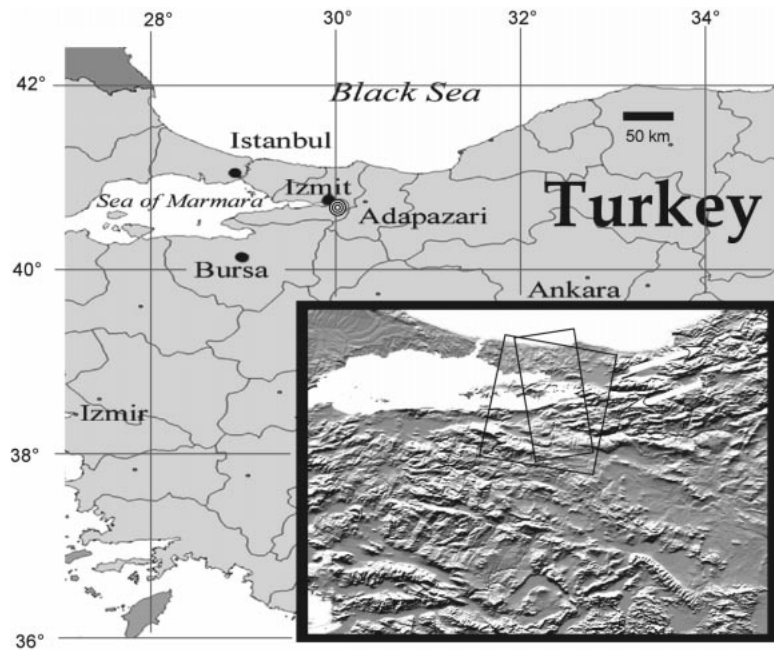

Figure 1. Map showing location of Kocaeli earthquake epicenter (concentric circles) in Turkey. Inset is shaded relief map of region showing that tectonic faulting and topography are highly correlated, and indicating that active faulting is dominant landscape-forming process at this scale. Right-lateral strike-slip North Anatolian fault is located between two white arrows in inset map and is topographically expressed as lineaments joining straight mountain fronts. Two boxes in inset show locations of LandSat and ERS-2 scenes over epicentral area and represent boundaries of images in Figure 2. Kocaeli earthquake was first called Izmit earthquake due to its proximity to city of Izmit.
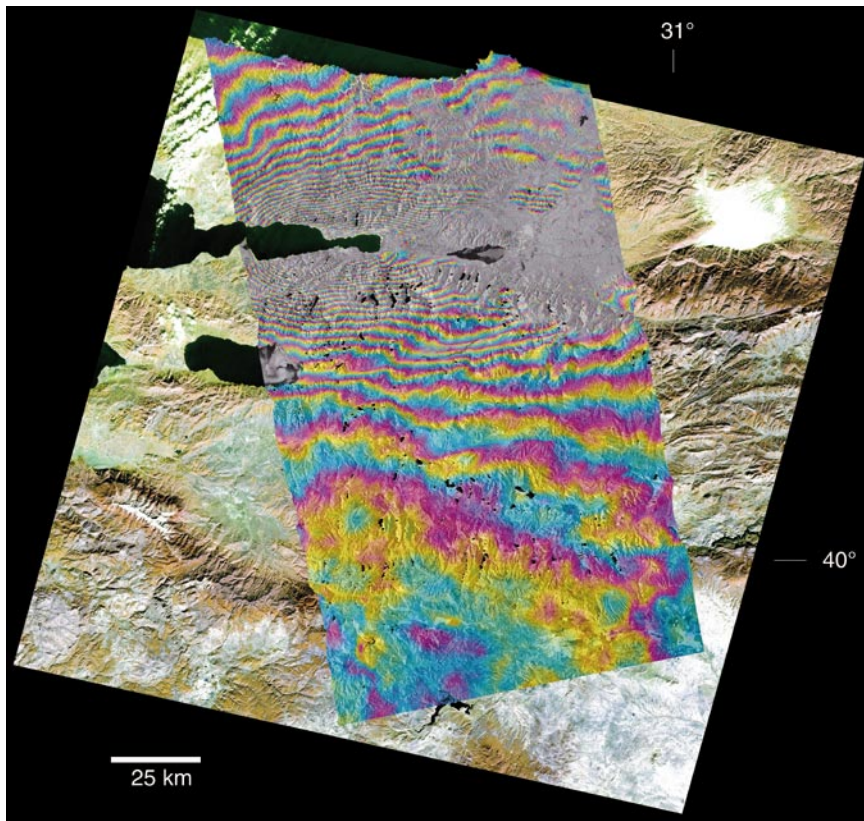
Figure 2. Synthetic aperture radar 2-pass interferogram mosaic overlaid on LandSat scene of epicentral area (Fig. 1). ERS-2 radar satellite scene was acquired on ascending pass, so radar was looking off to east, almost parallel to North Anatolian fault at edge of scene. Interferometric fringes represent change in distance between radar and ground in line of sight, or range distance. Each color cycle represents 2.83 cm of range distance change. Changes north of fault are away from satellite and changes south of fault are toward satellite. LandSat scene provides geographical and geological context for interferogram.
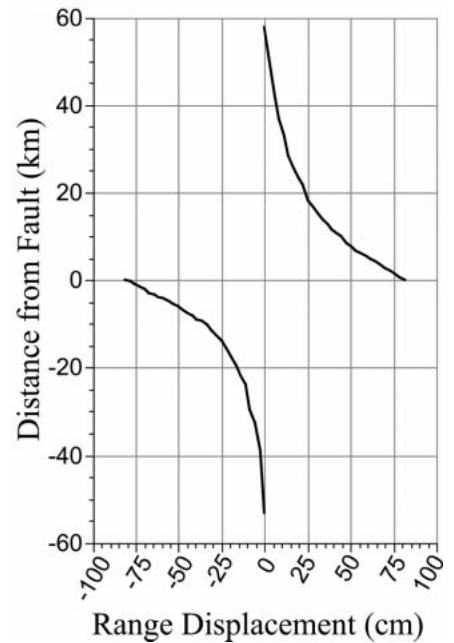

Figure 3. Range displacements measured on interferogram, north and south of North Anatolian fault. Maximum range displacement on this profile was about 2.1 m on either side, or total fault displacement of 4.2 m. Displacement continues for nearly 60 km on either side of fault at its maximum, although only ~50 km is recorded in this profile. Note that several fringes could not be resolved near fault and within body of water (dark area above Gölcük in Fig. 2).

2 data were acquired August 13, 1999, and September 17, 1999. The topographic signal was removed using a synthetic interferogram derived from a digital elevation model (DEM) based on digital terrain elevation level 1 data (DTED-1), with ~90 m posting. The specified horizontal accuracy of the DEM is ~130 m, and the linear vertical error is ~±30 m (Gesch, 1994). In two-pass InSAR, errors in the DEM are mapped into apparent deformation of the ground surface. This effect is characterized by a term called the altitude of ambiguity, which is the amount of topographic error required to generate one interferometric fringe in a topography-removed interferogram (Massonnet and Rabaute, 1993). For example, a 100 m DEM error would produce one spurious fringe in an interferogram with altitude of ambiguity of 100 m, or two spurious fringes in an interferogram with altitude of ambiguity of 50 m.

The SAR interferogram of the Kocaeli earthquake (Fig. 2) records the difference in range distance from the ERS-2 satellite to the ground in the radar line of sight before and after the earthquake. Subpixel cross-correla-

tion is used to register the pair of radar images. The interferogram, the actual fringes, can be computed for resolution elements, which are coherent between the two radar passes. Each fringe represents 2.83 cm of change in the radar line of sight caused by right-lateral slip along the North Anatolian fault. The range displacement (Fig. 3) measured perpendicular to the fault at Gölcük shows that deformation extended for ~50–60 km away from the fault, for a maximum total width of ~110 km, or almost equidimensional with the total fault-rupture length. The radar look direction during its ascending pass is approximately parallel to the fault. Thus the line of sight changes, shown by each fringe on the interferogram, are related to strain in a horizontal plane by the geometry of the look angle. The fault orientation varies through the scene and thus the simple assumption that the radar look direction and fault are parallel is not strictly valid. However, as a first approximation this is a reasonable simplification to apply for our data. The interferometric fringes can thus be used to determine the line of sight surface deformation associated with faulting

and strain release at the pixel-scale (20 m) resolution, at the centimeter or better precision, although there are potential error sources in these calculations.

Three major error sources in the interferogram are the DEM, orbital data, and atmospheric anomalies. We use a DEM in the two-pass InSAR processing. The altitude of ambiguity for this synthetic interferogram is ~1650 m, meaning that the error of DEM could contribute <1/20 of a fringe (2.83 cm line of sight deformation). The orbital data we used are from the precision orbit data product (PRC) provided by the German Processing and Archiving Facility (Massmann, 1995). The accuracy of the PRC position vectors is ~30 cm for along track and 8 cm for cross track (Massmann, 1995), which, in general, could contribute <3 cm of error in the InSAR-derived deformation map.

The third and probably the largest potential error source in our interferogram comes from the atmospheric delay anomaly (Zebker et al., 1997). The ERS-2 sensor orbits Earth at an altitude of ~790 km, and thus the electromagnetic wave from the sensor must propagate through the ionosphere, the stratosphere, and the troposphere. As a result, the radar pulses are subject to small variations in the

index of refraction along the line of propagation. Differences in the temperature, pressure, and water vapor content of the atmosphere between the two observation times can cause differences in the atmospheric path delay, which in turn introduce errors in the observed interferogram (Massonnet and Feigl, 1995; Lu et al., 2000). Wright et al. (2001) used the same ERS-2 data used in this study; they also used one ERS-1 data pair and found a difference of 3–4 fringes between the ERS-1 and ERS-2 interferograms. This difference is presumably caused by atmospheric delay anomalies in one or more of the four ERS-1/ERS-2 SAR images. We therefore believe that the amount of error caused by atmospheric delay anomaly in the ERS-2 interferogram is $<\sim10$ cm.

ELASTIC REBOUND

Perhaps one of the more enigmatic problems for earthquake prediction is knowing how and where the elastic strain energy that is ultimately released during an earthquake is stored. The modeling of large earthquakes based on continuum physics is difficult without knowing whether elastic strain is uniformly stored around a fault, compartmentalized along fault segments, or accumulating with unique spatial distributions for different faults. The distribution of elastic strain is important in both dimensions, i.e., vertically with depth and in the horizontal plane. For faults with simple stick-slip behavior, elastic strain accumulates across a fault over some finite width, $2b$ (also defined in Fig. 4, A and B). For example, for the 1906 San Francisco, California, earthquake, $b = 40$ km (Thatcher, 1975) and for the 1999 Manyi, Tibet, earthquake, $b = 40$ km (our interpretation of Peltzer et al., 1999). Assuming that the strain accumulates linearly with distance from the fault, we know that the fault strain at the end of the deforming zone, Δw, is ultimately related to the total strain accumulated over time (Fig. 4B). Simply, $\Delta w = 2b(\tau_s - \tau_d)/G$, where G is the shear modulus, τ_s is the static frictional shear stress, and τ_d is the dynamical frictional stress that exists at the initiation of a new earthquake cycle (Turcotte and Schubert, 1982). At some critical time, $t = t_c$, additional shear stress can no longer be transmitted across the fault and with this additional stress, the fault ruptures. The elastic energy that was stored in the $2b$ wide deformation zone is largely converted into seismic waves. If all of the stress is released, then Δw equals the fault displacement, d.

However, this simple view of elastic strain predicts a stress drop ($\tau_s - \tau_d$) associated with fault rupture that is too small for large earthquakes (Sornette, 1999), and therefore cannot be used to reliably answer the fundamental
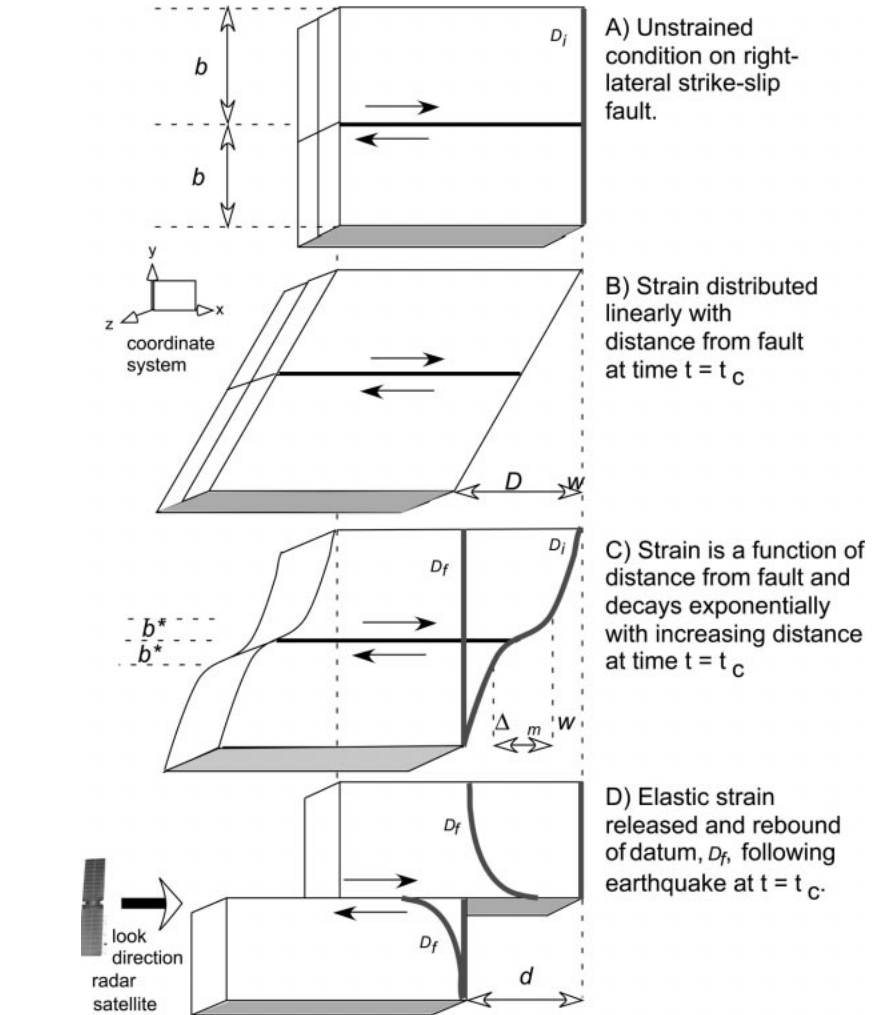

Figure 4. Models of elastic strain for right-lateral strike-slip fault like North Anatolian fault. A: Initial condition of crust in unstrained mode. We can use datum, D_i, to track elastic deformation of block. B: Linear strain model where rate of strain with distance is constant. Total recoverable strain for block $2b$ wide at critical condition is Δw. C: Nonlinear strain characterized by exponential decay of strain away from fault. Because most strain occurs over width much smaller than $2b$, it is useful to define effective strain width, $2b^*$. D_f is datum that records condition of strained block just prior to fault rupture, and D_i shows total strain that has accumulated. D: If all strain is released after faulting, D_i returns to its original unstrained shape and D_f becomes elastically deformed in manner that is mirror plane of deformed D_i at critical condition. D_f is equivalent to datum established just before faulting, which is exactly what repeat-pass synthetic aperture radar interferometry establishes.

question of where the strain is actually accumulating. Rheological inhomogeneity may account for this discrepancy, because geodetic inversions using elastic half-space models are sometimes difficult to reconcile with hypocentral depth observations (Segall and Davis, 1997). A commonly used visualization of elastic strain across a fault depicts nonlinear accumulation. A nonlinear accumulation of strain (Fig. 4C) around a fault can partially address the postearthquake stress drop because a significant amount of the total strain is stored in an effective width of $2b^*$, which is much smaller than the total strain width, $2b$. We define this effective width $2b^*$ based on

the distance over which a significant fraction (50%) of the strain was stored. Fault strain at the end of this narrower deforming zone defines Δw_m. There are few earthquakes for which a comparison can be made. For the 1906 San Francisco, California, earthquake, $b^* = 5$ km versus $b = 40$ km (Thatcher, 1975); for the 1999 Manyi, Tibet, earthquake, $b^* = 6$ km versus $b = 40$ km (our interpretation of Peltzer et al., 1999); and for the Kocaeli earthquake, $b^* = 10$ km versus $b = 60$ km (this paper).

For the Kocaeli earthquake, the relationship between the SAR interferogram and elastic rebound is as follows. Consider a linear surface
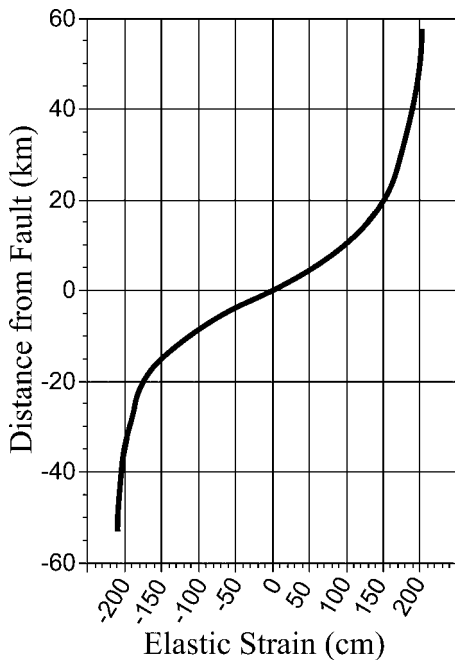
Figure 5. Reconstruction of elastic deformation for area north and south of North Anatolian fault just prior to Kocaeli earthquake, based on profile shown in Figure 3 but adjusted for radar look. This line is equivalent to datum D_i, in Figure 4C, just prior to rupture, and two other lines represent datum D_i, in Figure 4C, just after faulting.

datum, D_f, drawn perpendicular to a fault within a strained region just prior to strike-slip faulting (Fig. 4C). Another datum, D_i, represents a datum drawn perpendicular to the fault immediately after the previous earthquake. Following the next fault rupture, D_f will deform elastically, exactly recording the elastic rebound (Fig. 4D). After the faulting, D_f is essentially the mirror image of D_i. InSAR measures the positional changes of this datum D_i and is here used to document the elastic rebound for the Kocaeli earthquake.

Taking into account the radar look direction, and using the model of strain release shown in Figure 4, we reconstructed the pre-faulting strain at the critical condition along a single profile across the North Anatolian fault (Fig. 5). The total strain measured perpendicular to the fault at Gölcük (west of the epicenter), Δw, as determined by InSAR is ~4.2 m. This compares to a maximum displacement measured in the field of 5 m located 31 km east of the epicenter. Incoherence near the epicenter, probably from vegetation-cultivation changes, did not permit us to make a measurement there. The rupture of the North Anatolian fault on August 17, 1999, resulted in both sides of the fault rebounding elastically and releasing energy as elastic waves in the form of the Kocaeli earthquake. We suggest that the difference between D_f before and after

the earthquake is measured by InSAR and shows the elastic rebound resulting from the stress release accompanying the rupture.

We can deduce that the rebound is a function that is dependent on the distance from the fault and two important physical parameters, the depth of the earthquake and the shear modulus. However, we are not able to functionally separate these dependencies. Thus, a convenient way to express the strain or rebound as a function of distance on either side of the fault is by an exponential decay function of the form, $y = \beta_1 e^{\beta_2 x}$, where y is the amount of fault parallel deflection of a point at a distance x from the fault. For the Kocaeli earthquake this relationship can be estimated using regression, and results in parameter estimates of $\beta_1 = 2.12$ and $\beta_2 = -0.063$ in units of meters and kilometers, respectively. The β_1 term is the half-slip, the total slip is $2\beta_1$, measured at the fault and equivalent to Δw if all the strain is released. The second parameter, β_2, is related to the shear modulus and depth of faulting. For a given shear modulus, the shallower the faulting, the more rapid the decay with distance from the fault. For example, model estimates for β_2 are -0.04, -0.059, and -0.09, for hypocenters of 15 km, 10 km, and 6 km, respectively, using a shear modulus of 30 GPa.

DISCUSSION

The thrust of this paper is the demonstration that earthquake deformation mapping using InSAR may be directly related to elastic rebound for the Kocaeli earthquake. The InSAR–derived estimate of elastic rebound is subject to errors from atmospheric delay anomalies. The assumption that all of the deformation recorded is elastic may not be strictly valid, and there is also some evidence of aseismic deformation (Reilinger et al., 2000). However, this paper suggests that a fundamental question be posed. Is the amount of deformation that accumulated around the Kocaeli region characteristic of future earthquakes there, and if so, can InSAR be generally used to monitor this active fault and other active faults around the world in order to document regional strain accumulation for the purpose of earthquake prediction?

REFERENCES CITED
Barka, A., 1999, The 17 August 1999, Izmit earthquake: Science, v. 285, p. 1858–1859.
Gesch, D., 1994, Topographic data requirement for EOS global change research: U.S. Geological Survey Open-File Report 94-626, 60 p.
Lu, Z., Mann, D., Freymueller, J., and Meyer, D., 2000, Synthetic aperture radar interferometry of Okmok volcano, Alaska: Radar observations: Journal of Geophysical Research, v. 105, p. 10 791–10 806.
Massmann, F.H., 1995, Information for ERS PRL/PRC Users: GeoForschungsZentrum Potsdam Technical Note, 25 p.
Massonnet, D., and Feigl, K., 1998, Radar interferometry and its application to changes in the Earth's surface: Reviews of Geophysics, v. 36, p. 441–500.
Massonnet, D., and Rabaute, T., 1993, Radar interferometry: Limits and potentials: IEEE Transactions on Geoscience and Remote Sensing, v. 31, p. 455–464.
Peltzer, G., Crampe, F., and King, G., 1999, Evidence of nonlinear elasticity of the crust from the Mw 7.6 Manyi (Tibet) earthquake: Science, v. 286, p. 272–276.
Reilinger, R.E., Ergintav, S., Bürgmann, R., McClusky, S., Lenk, O., Barka, A., Gurkan, O., Hearn, L., Feigl, K.L., Cakmak, R., Aktug, B., Ozener, H., and Töksoz, M.N., 2000, Coseismic and postseismic fault slip for the 17 August 1999, M = 7.4, Izmit, Turkey earthquake: Science, v. 289, p. 1519–1524.
Rosen, P.A., Hensley, S., Zebker, H.A., Webb, F.H., and Fielding, E.J., 1996, Surface deformation and coherence measurements of Kilauea volcano, Hawaii, from SIR-C radar interferometry: Journal of Geophysical Research, v. 101, p. 109–123, 125.
Segall, P., and Davis, J.L., 1997, GPS applications for geodynamics and earthquake studies: Annual Reviews of Earth and Planetary Sciences, v. 25, p. 301–336.
Sornette, D., 1999, Earthquakes: From chemical alteration to mechanical rupture: Physics Reports, v. 313, p. 237–291.
Stein, R.S., Barka, A., and Dieterich, J.J., 1997, Progressive failure on the North Anatolian fault since 1939 by earthquake stress triggering: Geophysical Journal International, v. 128, p. 594–604.
Thatcher, W., 1975, Strain accumulation and release mechanism of the 1906 San Francisco earthquake: Journal of Geophysical Research, v. 80, p. 4862–4872.
Turcotte, D.L., and Schubert, G., 1982, Geodynamics—Applications of continuum physics to geological problems: New York, John Wiley & Sons, Inc., 422 p.
Wright, T.J., Fielding, E.J., Parsons, B.E., and England, P.C., 2001, Triggered slip: Observations of the 17 August 1999, Izmit (Turkey) earthquake using radar interferometry: Geophysical Research Letters (in press).
Zebker, H., Rosen, P., and Hensley, S., 1997, Atmospheric effects in interferometric synthetic aperture radar surface deformation and topographic maps: Journal of Geophysical Research, v. 102, p. 7547–7563.